ADVANCED BIOLOGY
www.advanced-bio.com

Spatiotemporal Control Over Protein Release from Artificial Cells via a Light-Activatable Protease

*Arjan Hazegh Nikroo, Wiggert J. Altenburg, Thijs W. van Veldhuisen, Luc Brunsveld, and Jan C. M. van Hest**

The regulation of protein uptake and secretion by cells is paramount for intercellular signaling and complex multicellular behavior. Mimicking protein-mediated communication in artificial cells holds great promise to elucidate the underlying working principles, but remains challenging without the stimulus-responsive regulatory machinery of living cells. Therefore, systems to precisely control when and where protein release occurs should be incorporated in artificial cells. Here, a light-activatable TEV protease (LaTEV) is presented that enables spatiotemporal control over protein release from a coacervate-based artificial cell platform. Due to the presence of Ni^{2+}-nitrilotriacetic acid moieties within the coacervates, His-tagged proteins are effectively sequestered into the coacervates. LaTEV is first photocaged, effectively blocking its activity. Upon activation by irradiation with 365 nm light, LaTEV cleaves the His-tags from sequestered cargo proteins, resulting in their release. The successful blocking and activation of LaTEV provides control over protein release rate and triggerable protein release from specific coacervates via selective irradiation. Furthermore, light-activated directional transfer of proteins between two artificial cell populations is demonstrated. Overall, this system opens up avenues to engineer light-responsive protein-mediated communication in artificial cell context, which can advance the probing of intercellular signaling and the development of protein delivery platforms.

1. Introduction

A fundamental feature to what makes cells "living" is their ability to communicate with one another, and to sense and modulate their surroundings. While cells employ various signaling modes to exchange information, one of their most universal forms of communication relies on diffusible signaling proteins.[1,2] During endocrine and paracrine signaling, sender cells release such molecules in response to perceived stimuli to initiate downstream signaling events in receiver cells, ultimately driving crucial collective biological functions that cannot be achieved by cells in isolation.[3,4] For example, multicellular organisms utilize diffusible cytokine-mediated information exchange to mount coordinated responses of immune cells against pathogens,[5,6] and to induce cellular differentiation and proliferation during tissue development and repair using growth factors,[7] with precise regulation over the timing, location, and extent of protein release. Engineering analogous stimulus-responsive control over the release of specific proteins holds great promise to probe the working principles of intercellular signaling on the molecular level. Highly notable successes in the engineering and modulation of cellular signaling in top-down fashion have been achieved, albeit that the chemical flexibility is limited by the complexity of living cells, the dense and interlinked nature of their signaling pathways, and interference by intra- and extracellular constituents needed to sustain life.[8–10]

Inspired by nature, the bottom-up engineering of artificial cells has over the years emerged as an exciting and orthogonal research area to reconstruct and study key cellular hallmarks in a well-controlled, life-like environment.[11–14] In order to understand how cells orchestrate their behaviors through intercellular signaling, significant progress has been made to incorporate aspects of cellular communication by engineering mechanisms to control the release and uptake of molecular cargo.[8] For example, multiple artificial cell designs with robust sender-receiver architectures,[15–18] bidirectional signaling systems,[19] signal amplification processes,[20] and the ability to communicate with living cells have been reported,[21–23] which typically

A. Hazegh Nikroo, W. J. Altenburg, T. W. van Veldhuisen, J. C. M. van Hest
Laboratory of Bio-Organic Chemistry
Department of Biomedical Engineering
and Institute for Complex Molecular Systems
Eindhoven University of Technology
P.O. Box 513, Eindhoven 5600 MB, The Netherlands
E-mail: j.c.m.v.hest@tue.nl

T. W. van Veldhuisen, L. Brunsveld
Laboratory of Chemical Biology
Department of Biomedical Engineering
and Institute for Complex Molecular Systems
Eindhoven University of Technology
P.O. Box 513, Eindhoven 5600 MB, The Netherlands

The ORCID identification number(s) for the author(s) of this article can be found under https://doi.org/10.1002/adbi.202400353

DOI: 10.1002/adbi.202400353

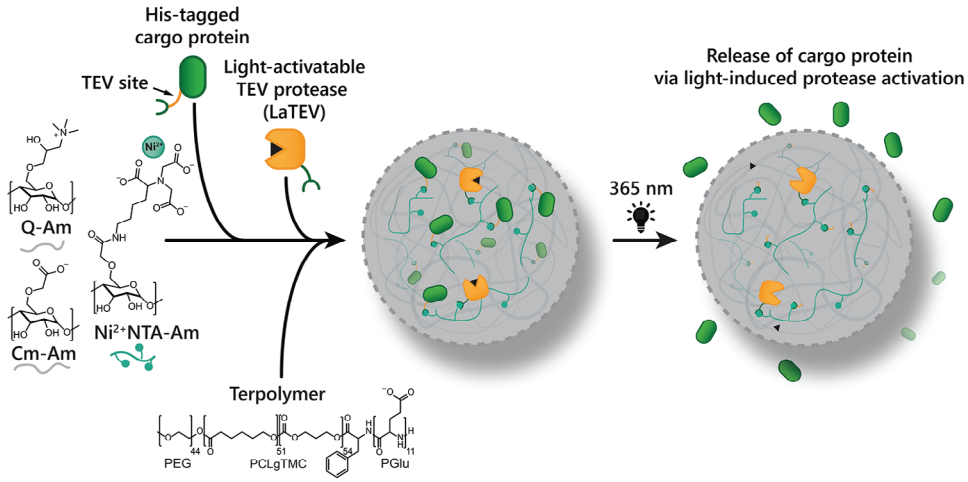

Figure 1. Schematic representation of coacervate assembly, loading of His-tagged proteins, light-triggered protease activation, and successive cargo protein release. Coacervates are formed by mixing positively charged quaternized amylose (Q-Am) with negatively charged carboxymethylated amylose (Cm-Am) and Ni^{2+} NTA functionalized amylose (Ni^{2+} NTA-Am). His-tagged protein cargo and light-activatable TEV protease (LaTEV) are loaded, after which terpolymer is added to stabilize the coacervate droplets. Illumination with 365 nm light activates LaTEV by liberating its active site cysteine from a photocaging moiety, in turn triggering cargo protein release through protease-mediated cleavage of the His-tag linkage.

employ the exchange of diffusible small signaling molecules over (semi)permeable compartment boundaries for information transfer. Though less abundantly integrated, especially when considering their key roles in natural cellular communication, proteins have also been utilized as signaling molecules in artificial cell contexts. Their release has been shown through among others cell-free protein synthesis,[24–26] vesicle fusion,[27] and compartment decomposition.[28,29] However, these systems generally lack stimulus-responsivity to regulate when and where protein release occurs. Without the intricate regulatory machinery of living cells, mechanisms to precisely control protein release from artificial cells should therefore be engineered to open up avenues toward communicative behavior that is more reminiscent of natural responsive protein-based signaling.

Among the repertoire of artificial cell platforms developed to date, coacervates have been gaining traction,[14,30] owing to their molecularly crowded matrix that mimics the densely packed internal milieu of living cells. In addition, they can be enclosed by semi-permeable membranes.[31–34] Liquid–liquid phase separated compartments have furthermore been shown to play a critical part in natural protein localization, highlighting their intrinsic ability to sequester proteins.[35] Despite these favorable properties, protein recruitment in coacervates is typically driven by preferential partitioning through charge complementarity with the coacervate matrix.[36–39] This mechanism is effective but challenging to control after sequestration, restricting possibilities for subsequent protein release. To address this, we previously reported the programmable uptake of His-tagged proteins in terpolymer-stabilized amylose-based coacervates through the incorporation of nitrilotriacetic acid-functionalized amylose complexed with Ni^{2+} (Ni^{2+}-NTA-Am).[40] By additionally inserting a protease cleavage site between the cargo protein and its His-tag, we demonstrated protein release through enzymatic cleavage by tobacco etch virus (TEV) protease. Notwithstanding, this approach is limited, as the TEV protease is directly active after uptake in the coacervates, resulting in cargo protein release from the moment of its addition. To achieve user-defined control over when and where protein release is triggered, this system should be made activatable with responsivity to an external cue. In this context, light is an attractive stimulus due to its high spatiotemporal control, allowing it to be focused on desired areas and delivered at any given time.

Herein, we report the integration of an engineered light-activatable TEV protease (LaTEV) in our terpolymer-stabilized coacervate artificial cell platform to establish light-triggered spatiotemporal control over cargo protein release (**Figure 1**). The system is based on the site-specific photocaging of the active-site cysteine in TEV protease, rendering the enzyme inactive until its decaging and activation is triggered upon exposure to 365 nm light. This property is exploited to enable effective light-activated enzymatic release of His-tagged cargo proteins, and to achieve spatial control through selective irradiation of a subset of the coacervate population. Moreover, we link LaTEV to a protein-protein interaction (PPI)-based uptake system in coacervates, displaying its general utility to design stimulus-responsive sender-receiver cell architectures. This work as such provides new opportunities toward the engineering of light-activatable coacervate-based artificial cell communication networks and synthetic protein delivery platforms.

2. Results and Discussion

2.1. Engineering a Light-Activatable TEV Protease (LaTEV)

In order to engineer LaTEV, we opted to replace the key active site Cys151 residue of TEV protease with a photocaged cysteine derivative that can be converted to a canonical cysteine using 365 nm light as activating stimulus. In our first approach, we opted to use protein engineering, following previous work by Nguyen et al., who reported the evolution of an orthogonal *Methanosarcina mazei* (Mm) PylRS / $tRNA_{CUA}$ pair for the genetic incorporation of the photocaged cysteine derivative

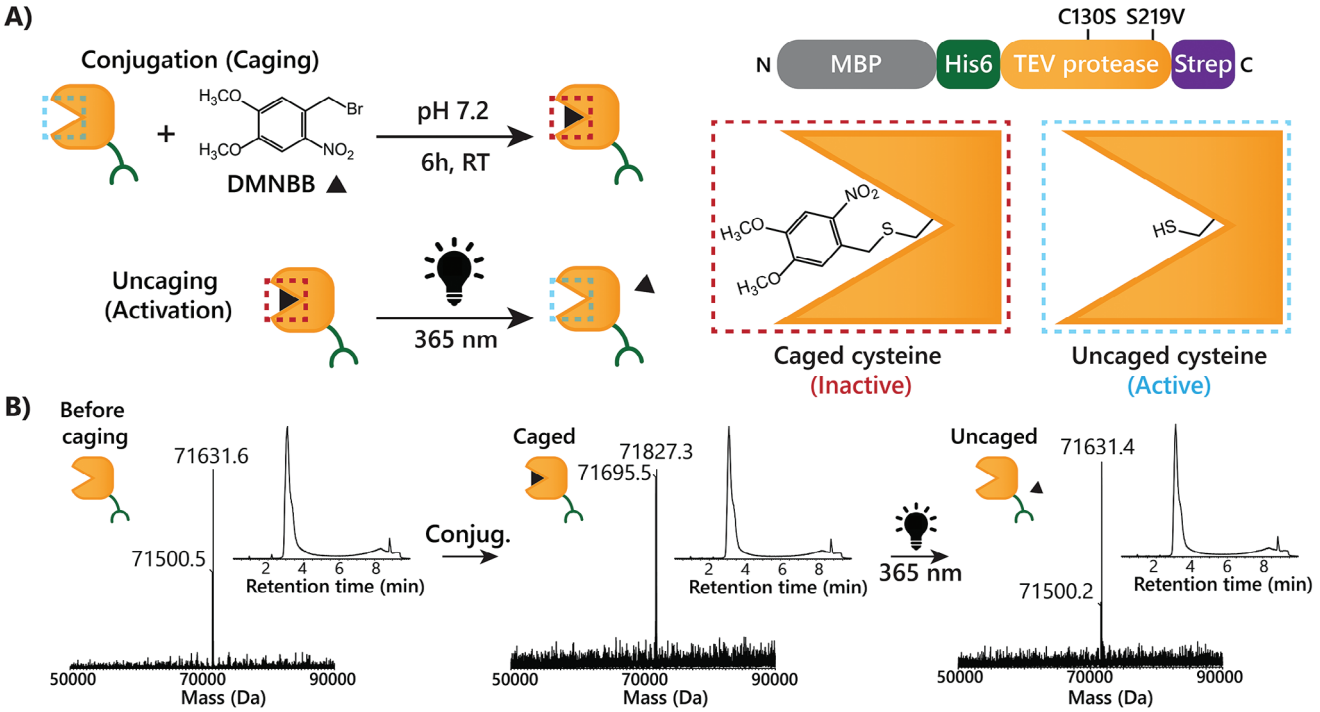

Figure 2. Production of LaTEV by photocaging MBP-TEV using DMNBB. A) Schematic representation of the protein construct design and mutations (top right), DMNBB conjugation to site-specifically photocage the active-site cysteine of MBP-TEV (top left), and the subsequent activation using 365 nm light to restore the active-site cysteine (bottom left). B) LC-MS Q-ToF analysis of MBP-TEV before and after conjugation, and after uncaging with 365 nm light. Deconvoluted mass spectra are shown with the total ion count chromatogram as inlay. Expected masses: 71500.8 Da and 71631.9 Da (uncaged protein), 71696.0 Da and 71827.1 Da (caged protein). For both states, the lower mass can be ascribed to excision of the N-terminal methionine in *E. coli* (-131 Da).

4,5-methylenedioxy-2-nitrophenylethyl-L-cysteine (MDNPE-Cys) in TEV protease via amber codon suppression.[41] We therefore synthesized MDNPE-Cys (Figures S1 and S2, Supporting Information), introduced an amber stop codon in TEV protease to exchange Cys151 with MDNPE-Cys, and implemented a Ser219Val mutation to abrogate protease self-cleavage.[42] In addition, an N-terminal maltose binding protein (MBP) domain was incorporated to enable overexpression and storage with enhanced solubility, while His- and Strep tags were included at the N- and C-termini of the protein, respectively, to enable purification of the full-length protein. The non-cleavable His-tag furthermore introduced affinity of LaTEV for coacervates containing Ni^{2+}-NTA functionalized amylose.

Expression of LaTEV was performed in *E. coli*, co-transformed with the orthogonal Mm PylRS / $tRNA_{CUA}$ pair, with MDNPE-Cys supplemented in the dark. Purification via Ni^{2+}-NTA and Strep-Tactin affinity chromatography afforded the pure protein in an overall yield of 0.2 mg L^{-1} culture medium, as confirmed by SDS-PAGE analysis (Figure S3, Supporting Information). The relatively low yield was a result of the expression of truncation products that were effectively removed via Strep-Tactin affinity chromatography. Subsequent evaluation of protein identity via liquid chromatography quadrupole time of flight mass spectrometry (LC-MS Q-ToF) revealed the presence of both uncaged protease and the expected photocaged protease, which indicated incomplete protease caging (Figure S3, Supporting Information). Since the incorporation of a canonical cysteine at position 151 was deemed unlikely due the amber codon suppression system, this might be attributed to partial cleavage of the nitrophenyl group in MDNPE-Cys upon exposure to light, despite efforts to perform protein expression, extraction, and purification in the dark.

To address the apparent incomplete caging, we next explored whether the covalent conjugation of a photocaging moiety to Cys151 after protein expression would represent an alternate method to produce LaTEV. The commercially available photocaging compound 4,5-dimethoxy-2-nitrobenzylbromide (DMNBB) was selected for this approach, as it can covalently bind the sulfhydryl group of accessible cysteine residues via its bromomethyl group and can readily be removed upon illumination with 365 nm light (**Figure 2A**).[43] Since amber codon suppression was not required for this methodology, we anticipated the protein expression yield to be higher. Moreover, conjugation with DMNBB only requires protection from light from the conjugation step onward, allowing straightforward protein expression and purification without risk of premature decaging. As a potential disadvantage of the chemical caging strategy however, multiple cysteines in TEV protease besides active-site Cys151 could be modified with DMNBB (Cys19, Cys110, Cys130). Based on previous reports and the crystal structure of TEV protease, we anticipated that Cys151 and the surface-exposed Cys130 would be susceptible to DMNB-treatment, whereas Cys19 and Cys110 are buried in the folded protein structure and hence inaccessible (Figure S4,

Supporting Information).[44,45] As such, we introduced a stabilizing Cys130Ser mutation that was previously reported by Correnti et al. to enable the site-specific DMNBB-conjugation at the active site cysteine.[46] The resulting fusion protein featuring the canonical Cys151 residue was expressed in *E. coli* and purified via Ni^{2+}-NTA and Strep-Tactin affinity chromatography, with a yield of ≈15 mg L^{-1} culture medium, as confirmed via SDS-PAGE and LC-MS Q-ToF (Figure S5, Supporting Information; Figure 2B).

After purification, we incubated the protein with tris(2-carboxyethyl)phosphine (TCEP) for 20 min as preparative reduction step prior to conjugation, after which the reducing agent was removed via buffer exchange to avert reactivity with DMNBB. We next performed the DMNB-conjugation by incubation with 15 molar equivalents of DMNBB for 6 h in the dark. Following a second buffer exchange to remove unreacted compound, LC-MS Q-ToF analysis revealed two peaks representative of DMNB-conjugated protein, corresponding to the full-length protein and the protein deprived of its N-terminal methionine due to methionine aminopeptidase processing in *E. coli*.[47] Importantly, masses indicative of unconjugated protein could not be identified in the deconvoluted mass spectrum, implying a (near) complete DMNB-conjugation (Figure 2B). Subsequent LC-MS Q-ToF analysis following a preliminary irradiation test with 365 nm light (0.21 mW cm^{-2}, 15 min) proved that the DMNB moiety could effectively be cleaved to attain the uncaged protease with its cysteine residue restored.

2.2. Characterization of LaTEV with a FRET Reporter Protein

To verify the activity of LaTEV in its caged and light-activated state, we designed and expressed an mNeonGreen-mCerulean (mNG-mCE) reporter fusion protein, featuring a flexible GGS linker with a TEV protease cleavage site (ENLYFQ▼S) (Figure S6, Supporting Information). The fusion protein exhibits a high Förster resonance energy transfer (FRET) efficiency when the cleavable linker is intact, with mCE in close proximity of mNG. Conversely, linker cleavage by activated LaTEV leads to a decrease in FRET due to loss of proximity of mCE and mNG, allowing the fusion protein to report on the activity of LaTEV before and after irradiation (**Figure** 3A).

As an initial test, 100 nM of LaTEV was irradiated with 365 nm light (0.21 mW cm^{-2}, 1 min), after which 500 nM of mNG-mCE was added, and FRET was monitored for 16 h. This brief illumination successfully triggered the protease activation and cleavage of mNG-mCE over time, as evidenced by a concomitant gradual loss of FRET from mCE to mNG. Evidently, cleavage of mNG-mCE only occurred upon incubation with LaTEV that was exposed to 365 nm light, as the FRET signal remained virtually unaltered upon incubation with LaTEV that was kept in the dark (Figure 3B). This demonstrates the absence of background protease activity of LaTEV in the photocaged state and is as such in line with the implied (near) complete conjugation as determined via LC-MS Q-ToF analysis (Figure 2B).

With light being a tunable stimulus, we next examined whether LaTEV activity could be regulated by varying the irradiation time. As expected, LaTEV samples irradiated for 5 and 10 min revealed a more rapid decrease in FRET over time as compared to 1 minute irradiation, signifying a more effective protease activation (Figure 3B). The difference between irradiation for 5 and 10 min was less pronounced, indicating that 5 min of irradiation yields near-complete decaging. The activation of LaTEV could analogously be regulated by adjusting the laser power, with a decrease in laser power yielding a more gradual protease activation relative to full laser power (Figure S8, Supporting Information). Next, we calculated the relative FRET efficiency to assess the extent of mNG-mCE cleavage. To this end, mNG and mCE were expressed individually and mixed to generate a relative FRET efficiency that would be obtained upon complete cleavage of mNG-mCE. Irradiation for 5 and 10 min led to quantitative cleavage, with their respective FRET efficiencies of 0.500 and 0.496 in good agreement with the FRET efficiency of 0.488 for the individual mixture after 16 h (Figure 3C). Finally, comparison to constitutively active MBP-TEV revealed LaTEV to exhibit a lower activity at equal concentration, with a 1.11-fold higher relative FRET efficiency after 4 h of incubation, irrespective of irradiation time (Figure S9, Supporting Information). This apparent incomplete recovery of activity might be attributed to partial denaturation of the enzyme during the conjugation procedure. Despite this, the highly effective caging and functional light-triggerable activation of LaTEV in bulk, without background activity, provided us with a suitable activable enzyme for usage in our artificial cell platform.

2.3. Light-Activated Enzymatic Cargo Protein Release from Coacervates

We next set out to integrate LaTEV in coacervates to establish a light-activatable enzymatic protein release mechanism. For this purpose, a superfolder green fluorescent protein with a TEV protease-cleavable His-tag (sfGFP-His) was selected as model cargo protein (Figure S10, Supporting Information). sfGFP is normally excluded from the coacervates, unless its recruitment is enforced through the interaction between its His-tag and the incorporated Ni^{2+}-NTA-Am.[40] Proteolytic cleavage of the His-tag following uptake should as such result in protein release due to a loss of affinity for the coacervate matrix (**Figure** 4A).

To assess whether 365 nm light is capable of triggering LaTEV-mediated protein cargo release, we prepared terpolymer-stabilized coacervates in a 2:0.8:0.2 charge ratio of quaternized amylose (Q-Am), carboxymethylated amylose (Cm-Am), and NTA-Am, respectively, which was previously shown to yield coacervate droplets that effectively recruit His-tagged cargo proteins.[40] The terpolymer membrane stabilizes the coacervates and is dynamic and semipermeable to proteins.[33] The coacervates were co-loaded using 100 nM of sfGFP-His and 40 nM of His-tagged LaTEV, and irradiated with 365 nm light (0.21 mW cm^{-2}, 5 min) or left in the dark. We subsequently monitored the sfGFP fluorescence intensity in the coacervate matrices over 16 h using confocal microscopy. Gratifyingly, irradiated co-loaded coacervates exhibited a clear release of sfGFP, as illustrated by a significant decrease in fluorescence intensity in the coacervate matrices over time (Figure 4B, fourth row), which was quantified for the resulting micrographs (Figure 4C). Importantly, the observed fluorescence intensity decrease could be attributed to protease-mediated release of sfGFP, and not to photobleaching

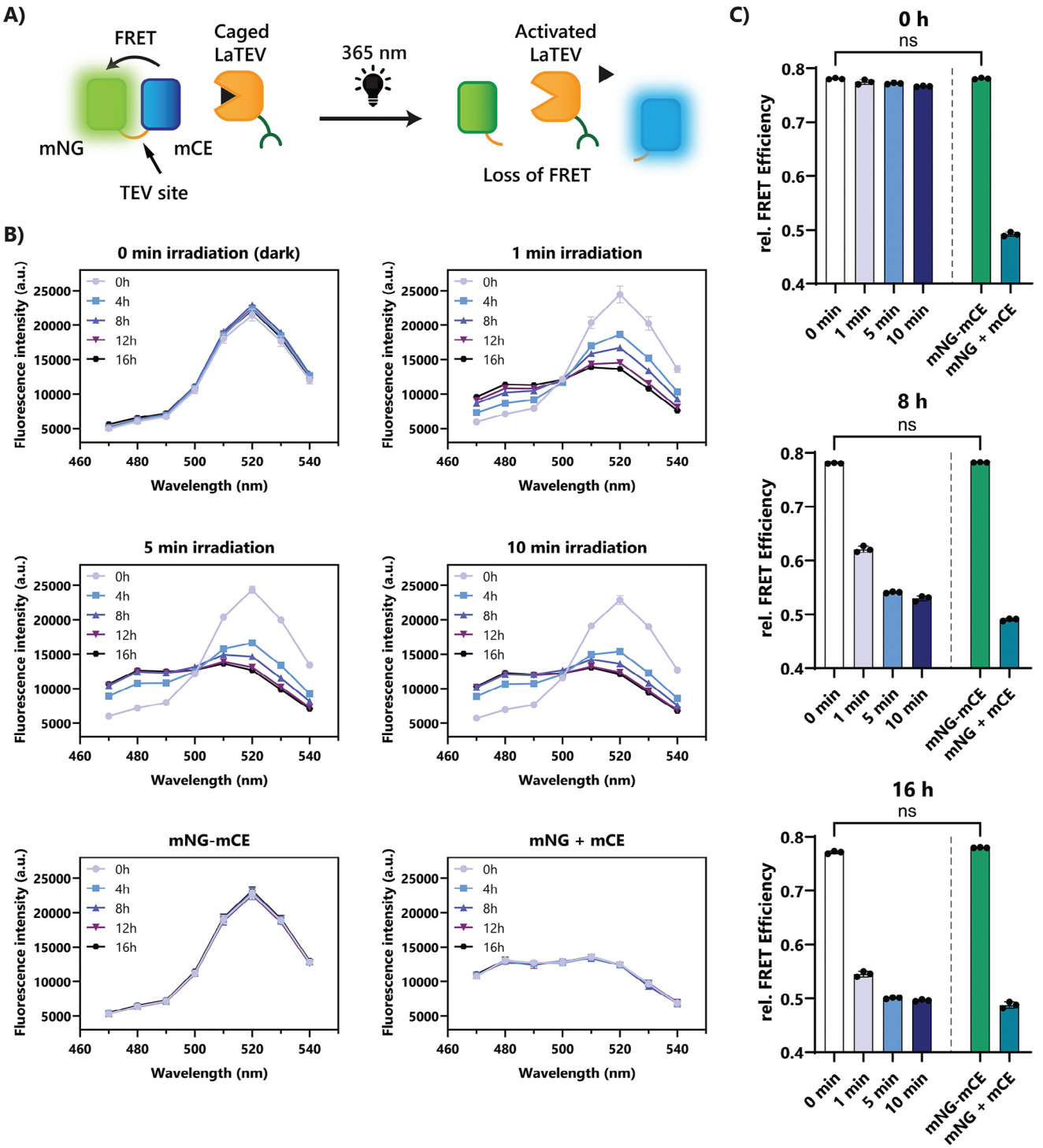

Figure 3. Characterization of LaTEV activity in caged and uncaged state with a fusion protein-based FRET reporter. A) Schematic representation of LaTEV activation and FRET readout. Irradiation of LaTEV with 365 nm light liberates the protease active site. This enables it to cleave the mNeonGreen-mCerulean fusion protein linkage, resulting in a decrease in FRET. B) Fluorescence intensity spectra of the fusion protein reporter (500 nM) were measured in the presence and absence of LaTEV (200 nM). Samples were irradiated for 1, 5, or 10 min with 365 nm light and FRET was monitored over time ($N = 3$). C) The relative FRET efficiency was calculated via Equation S1 (Supporting Information) using donor (mCE) fluorescence intensity at 480 nm and acceptor (mNG) fluorescence intensity at 520 nm. Data points represent individual measurements. Statistical evaluation for 0 min and mNG-mCE was performed via a one-way ANOVA test, as indicated by ns (not significant, $p > 0.05$).

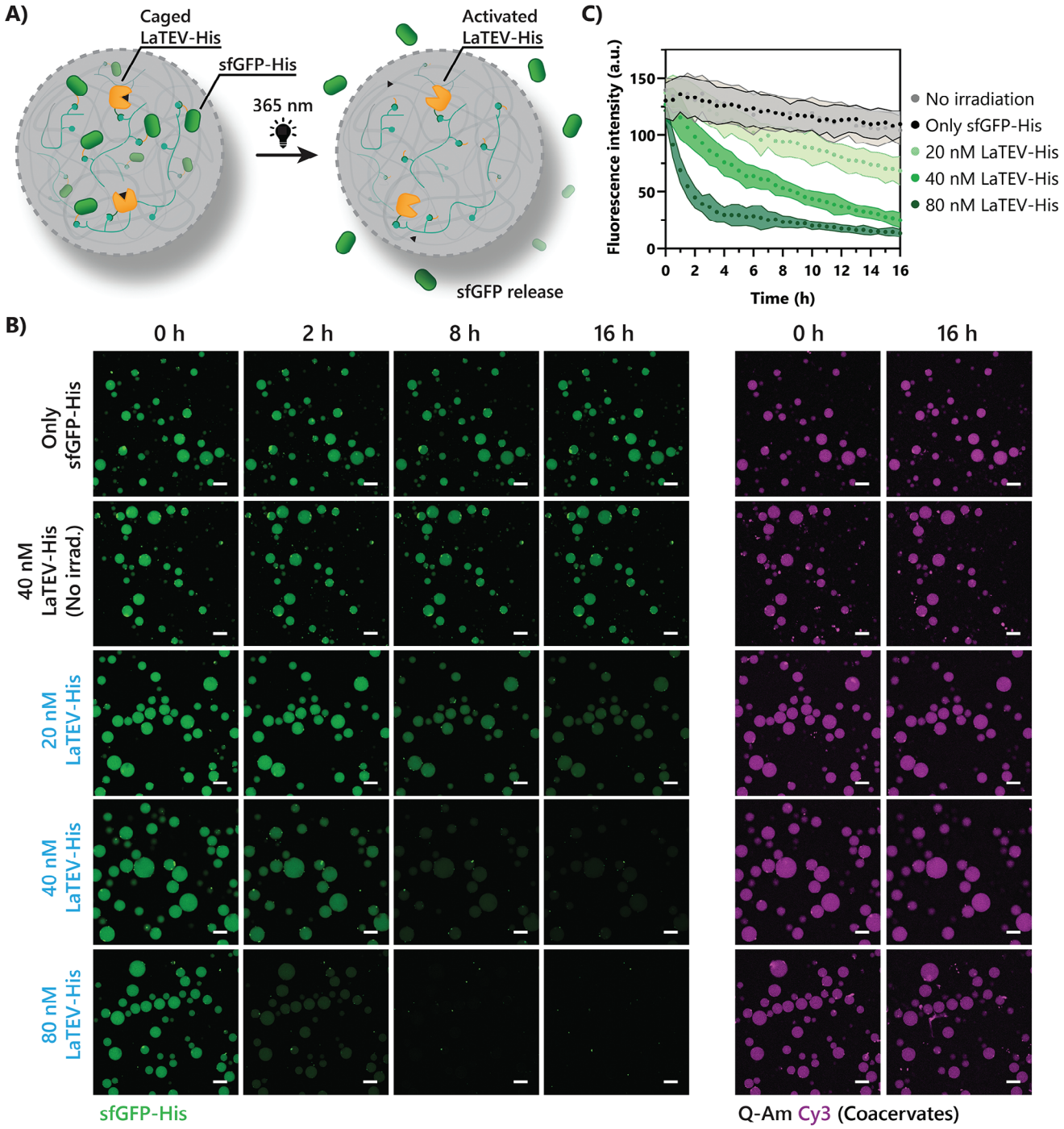

Figure 4. Light-activated control over enzymatic protein release from coacervate-based artificial cells. A) Schematic overview of light-triggered activation of His-tagged LaTEV and successive sfGFP cargo release. B) Confocal micrographs over time showing coacervates harboring sfGFP-His (100 nM, green) and varying concentrations of LaTEV (0–80 nM) following irradiation with 365 nm light for 5 min. Cy3-labeled Q-Am (magenta) was added to visualize the coacervate droplets. C) Quantification of mean sfGFP fluorescence intensity in coacervates over time. Data represents mean ± standard deviation. $N \geq 30$.

of sfGFP by the 365 nm laser, since a similar decrease in intensity was not observed following irradiation of sfGFP-loaded coacervates (Figure 4B, first row) or coacervates loaded with LaTEV and sfGFP-His lacking a TEV protease cleavage site (Figure S13, Supporting Information). Without irradiation, coacervates containing both sfGFP-His and LaTEV exhibited no substantial decrease in sfGFP fluorescence intensity, testifying to the effective caging and inactivation of LaTEV (Figure 4B, second row). The subtle decrease in mean sfGFP fluorescence intensity over time for this sample can be ascribed to photobleaching during the

measurement, with sfGFP-loaded coacervates also displaying a similar decrease (Figure 4C).

Upon further evaluation of light-activated sfGFP cargo release using 20 and 80 nM of LaTEV, we observed a LaTEV concentration-dependent release of sfGFP cargo. For 80 nM of LaTEV, a substantially decreased sfGFP fluorescence intensity could already be measured at ≈2 h (Figure 4B, fifth row and Figure 4C), relative to the initially observed sfGFP release for 40 nM of LaTEV. Conversely, a more gradual cargo release was observed for 20 nM of LaTEV, with release still ongoing at the 16 h timepoint (Figure 4B, third row and Figure 4C). The ability to activate and tailor the gradual release of protein could be ideal for contexts in which release over a span of hours or days is required, rather than rapid burst release, for instance to carefully elicit a desired output in living cells with biofunctional protein cargo.

A major advantage of light over other stimuli is that it can be applied in a spatially controlled manner. To demonstrate this level of control, we sought to selectively trigger cargo protein release in a coacervate subset. To this end, we prepared coacervates co-loaded with 100 nM of sfGFP-His and 40 nM of His-tagged LaTEV, and applied a partial cover that prevents the passage of incident light to one half of the microscopy slide containing the coacervates (**Figure 5A**). The sample was then irradiated with 365 nm light (0.21 mW cm^{-2}, 5 min), after which sfGFP fluorescence in the coacervates was monitored through confocal microscopy over time. Following incubation for 16 h in the dark, sfGFP fluorescence was found to be maintained in coacervates located within the area that was protected from incident light, indicating the retention of cargo protein in this coacervate population as a result of LaTEV inactivity. By contrast, coacervates that were exposed to 365 nm light displayed an effective release of sfGFP over time as a result of LaTEV activation, as could be observed after 4 and 16 h in the resulting micrographs (Figure 5B,C), and quantified in the exposed coacervates relative to the covered coacervates (Figure 5D). These results therefore demonstrate that protein cargo can be released from a specific coacervate subset through spatially selective activation of LaTEV.

2.4. Light-Activated Transfer of Protein Cargo Between Coacervate Populations

To highlight the utility of LaTEV in an artificial cell context, we designed a unique light-activatable sender-receiver cargo transfer system by integrating LaTEV with PPI-based recruitment using two artificial cell populations. Specifically, a "sender" population was prepared by co-loading coacervates using 40 nM of His-tagged LaTEV and 100 nM of His-tagged sfGFP-cRaf_pS233/pS259 cargo protein (sfGFP-cRaf-His; Figure S15, Supporting Information). The latter protein is composed of sfGFP with a TEV protease cleavable His-tag, fused to a doubly phosphorylated peptide derived from cRaf, which is capable of specifically binding dimeric 14-3-3 scaffold proteins through a bivalent interaction with nanomolar-range affinity.[48–50] A "receiver" population was prepared and loaded with 100 nM of DyLight650-labeled His-tagged tobacco 14-3-3 protein (T14-3-3-His). We anticipated that the light-triggered activation of LaTEV would enable it to cleave the His-tag from the sfGFP-cRaf cargo protein in the sender coacervate population, thereby facilitating its release. The released sfGFP-cRaf protein, without His-tag, would then diffuse through the bulk until it would be recruited by a receiver cell through specific T14-3-3-dependent affinity-based sequestration (**Figure 6A**). Following the initial mixing of the protein-loaded sender and receiver populations, confocal microscopy analysis indeed confirmed the sfGFP-cRaf-His and T14-3-3-His proteins to reside in separate coacervate populations, as evidenced by the lack of overlap of sfGFP and DyLight650 fluorescence (Figure 6B; top row and Figure 6C; left column). To subsequently demonstrate the light-activated directional cargo transfer, we irradiated the mixture with 365 nm light (0.21 mW cm^{-2}, 5 min), after which the sample was incubated in the dark for 12 h. As anticipated, re-evaluation of the samples revealed a clear release of sfGFP-cRaf from the sender population. In addition, the receiver coacervates containing T14-3-3-His displayed a significant increase in sfGFP fluorescence intensity relative to the initial timepoint, confirming the effective transfer of cargo protein (Figure 6B; middle row and Figure 6C; middle column). Importantly, for an equivalent sample that was not exposed to 365 nm light, no substantial sfGFP-cRaf release was observed from the sender population, although a small amount of the protein was found to be present in the receiver population (Figure 6B; bottom row and Figure 6C; right column). With LaTEV kept inactive, this might be ascribed to partitioning of sfGFP-cRaf that remained in the bulk solution. These results as such demonstrate that LaTEV can be integrated with other coacervate uptake methods to establish controllable protein-based signaling from one artificial cell population to another, which could be applied to study life-life communication pathways in an artificial cell context.

3. Conclusion

In summary, we have engineered a light-activatable TEV protease, LaTEV, and integrated it into an artificial cell platform to establish responsive control over enzymatic release of protein cargo. Our approach relies on the site-selective photocaging of the active-site cysteine in TEV protease using compound DMNBB, which impedes protease activity until LaTEV is uncaged upon brief exposure to 365 nm light. A FRET assay using an engineered fusion protein reporter demonstrated the caging of LaTEV, without background activity, and proved that irradiation with 365 nm light successfully restores LaTEV's ability to cleave substrate protein. By incorporating LaTEV into a coacervate-based artificial cell platform that utilizes the Ni^{2+}-NTA/His-tag interaction for protein uptake, we established an activatable protein release system, demonstrating the effective release of sfGFP proteins from the coacervate core through light-activated enzymatic cleavage of their His-tags. This regulatory mechanism provided control over cargo release rate and enabled the triggerable protein release from specific coacervates via selective irradiation. Besides demonstrating protein release to the bulk, also a synthetic sender-receiver system was constructed that enables stimulus-responsive directional shuttling of protein cargo from one artificial cell population to another. For this purpose, LaTEV was combined with a PPI-mediated recruitment system based on the scaffold protein 14-3-3 and an interacting peptide module. Overall, this work provides a generally applicable and versatile light responsive cargo protein release system, with the potential to

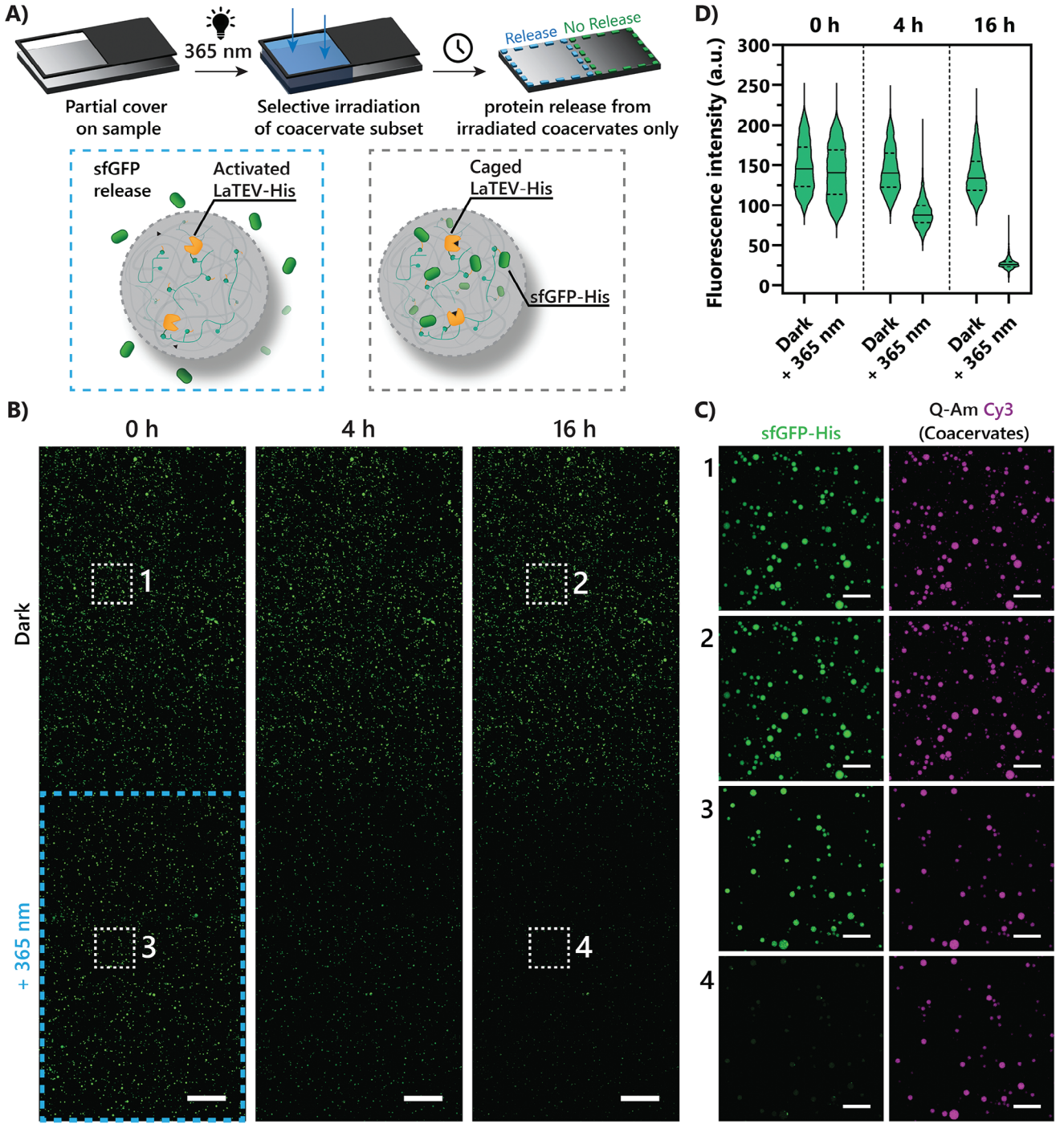

Figure 5. Spatial control over enzymatic protein release by selective activation of LaTEV in a coacervate subset. A) The cover protects coacervates in one section from 365 nm light and enables irradiation of coacervates in the other section. B) Confocal micrographs of coacervates containing sfGFP-His (100 nM, green) and His-tagged LaTEV (40 nM). The blue frame encloses the irradiated section. The white boxes enclose sections for which magnifications are shown in panel C). Cy3-labeled Q-Am (magenta) was added to visualize coacervates. D) Quantification of sfGFP fluorescence intensity in coacervates that were kept in the dark or exposed to 365 nm light. Solid lines inside the violin plot represent the median, and dashed lines represent the upper and lower quartiles. $N \geq 1500$. Scale bars: 300 µm (panel B) and 50 µm (panel C). Uncropped micrographs of the Cy3 channel are provided in Figure S14, Supporting Information.

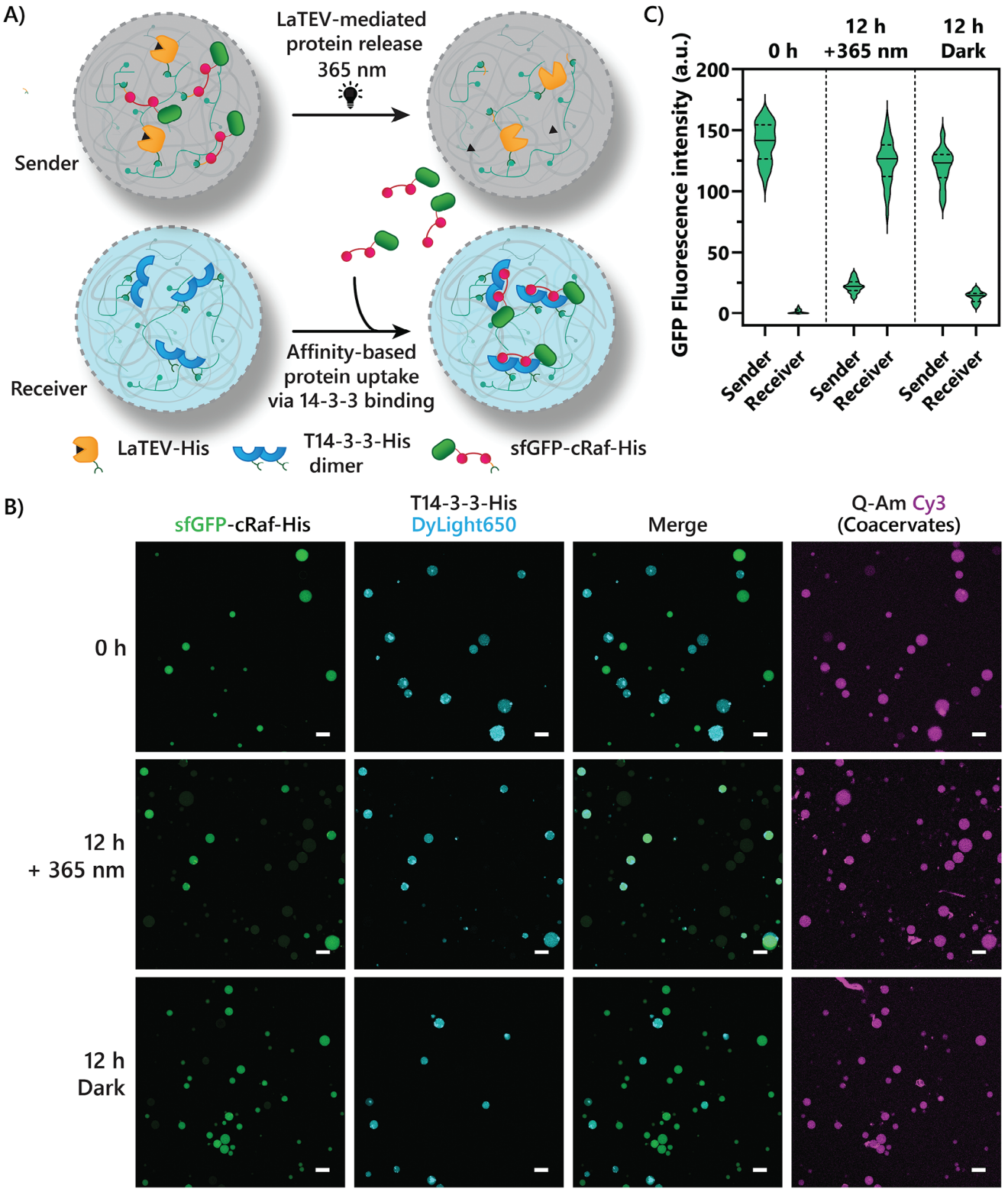

Figure 6. Light-activated protein transfer between two coacervate populations. A) Triggered transfer of sfGFP-cRaf fusion protein to a receiver population based on affinity for 14-3-3 protein. B) Confocal micrographs of "sender" coacervates loaded with sfGFP-cRaf-His (100 nM, green) and His-tagged LaTEV (40 nM) with "receiver" coacervates containing T14-3-3-His (100 nM, cyan) at 0 and 12 h after exposure to 365 nm light for 5 min or complete incubation in the dark (Dark). Cy3-labeled Q-Am (magenta) was added to visualize coacervates. C) Quantification of sfGFP fluorescence intensity in coacervate sender and receiver populations. The solid lines inside the violin plot represent the median. Dashed lines represent the upper and lower quartiles. $N \geq 15$. Scale bars: 15 µm.

design, control, and study light-responsive protein-based signaling pathways in an artificial cell context.

Apart from utility in a fully artificial context, we anticipate LaTEV could be adopted to introduce stimulus-responsive spatiotemporal control over protein release to establish communication between artificial and living cells in the future. While dependent on irradiation with 365 nm light to trigger protein release in its current iteration, photocaging compounds with responsivity to longer wavelengths could be introduced to utilize more biocompatible visible or near-infrared light sources, which can be important for translation to a context with living cells. Growth factors and cytokines with cleavable His-tags might enable LaTEV-equipped coacervates to be adopted as protein release platform for controlled cargo delivery in tissue engineering applications, with precise control over cargo release at specific target sites upon irradiation. Similarly, the conjugation-based photocaging strategy may prove useful to engineer other light-activatable enzymes to impart further controllability in artificial cells, in view of many enzymes possessing a cysteine proximal to or as part of their active-site catalytic triad.[51]

Supporting Information

Supporting Information is available from the Wiley Online Library or from the author.

Acknowledgements

The Dutch Ministry of Education, Culture, and Science is acknowledged for funding (Gravitation Programs 024.001.035, 024.005.020, and the Spinoza premium 72–259). Joost van Dongen and Sebastian van den Wildenberg are acknowledged for their help with LC-MS Q-ToF measurements. Yvonne van Mil is thanked for cloning the mNG-mCE FRET reporter construct and providing mNG and mCE.

Conflict of Interest

The authors declare no conflict of interest.

Author Contributions

A.H.N. designed and performed the experiments and analyzed the results. W.J.A. and T.W.V. performed experiments related to the initial genetic incorporation strategy. L.B. provided conceptual input. J.C.M.H. conceived and supervised the study. A.H.N. wrote the manuscript with input from the other authors.

Data Availability Statement

The data that support the findings of this study are available from the corresponding author upon reasonable request.

Keywords

artificial cells, coacervates, liquid-liquid phase separation, photoswitchable proteins, scaffold proteins, TEV protease

Received: June 20, 2024
Revised: September 11, 2024
Published online: September 27, 2024

[1] J. A. Ramilowski, T. Goldberg, J. Harshbarger, E. Kloppman, M. Lizio, V. P. Satagopam, M. Itoh, H. Kawaji, P. Carninci, B. Rost, A. R. R. Forrest, *Nat. Commun.* **2015**, *6*, 7866.
[2] R. Lentini, N. Yeh Martín, S. S. Mansy, *Curr. Opin. Chem. Biol.* **2016**, *34*, 53.
[3] E. Armingol, A. Officer, O. Harismendy, N. E. Lewis, *Nat. Rev. Genet.* **2021**, *22*, 71.
[4] S. Toda, N. W. Frankel, W. A. Lim, *Curr. Opin. Chem. Biol.* **2019**, *52*, 31.
[5] S. S. Chavan, V. A. Pavlov, K. J. Tracey, *Immunity* **2017**, *46*, 927.
[6] G. Altan-Bonnet, R. Mukherjee, *Nat. Rev. Immunol.* **2019**, *19*, 205.
[7] S. Werner, R. Grose, *Physiol. Rev.* **2003**, *83*, 835.
[8] H. Karoui, P. S. Patwal, B. V. V. S. Pavan Kumar, N. Martin, *Front. Mol. Biosci.* **2022**, *9*, 880525.
[9] A. O. Robinson, O. M. Venero, K. P. Adamala, *Curr. Opin. Chem. Biol.* **2021**, *64*, 165.
[10] J. M. Smith, R. Chowdhry, M. J. Booth, *Front. Mol. Biosci.* **2022**, *8*, 809945.
[11] E. Rideau, R. Dimova, P. Schwille, F. R. Wurm, K. Landfester, *Chem. Soc. Rev.* **2018**, *47*, 8572.
[12] B. C. Buddingh, J. C. M. Van Hest, *Acc. Chem. Res.* **2017**, *50*, 769.
[13] C. Guindani, L. C. da Silva, S. Cao, T. Ivanov, K. Landfester, *Angew. Chem., Int. Ed.* **2022**, *61*, e202110855.
[14] A. B. Cook, S. Novosedlik, J. C. M. van Hest, *Acc. Mater. Res.* **2023**, *4*, 287.
[15] T. Y. D. Tang, D. Cecchi, G. Fracasso, D. Accardi, A. Coutable-Pennarun, S. S. Mansy, A. W. Perriman, J. L. R. Anderson, S. Mann, *ACS Synth. Biol.* **2018**, *7*, 339.
[16] K. P. Adamala, D. A. Martin-Alarcon, K. R. Guthrie-Honea, E. S. Boyden, *Nat. Chem.* **2017**, *9*, 431.
[17] T. Chakraborty, S. V. Wegner, *ACS Nano.* **2021**, *15*, 9434.
[18] E. Magdalena Estirado, A. F. Mason, M. Á. Alemán García, J. C. M. Van Hest, L. Brunsveld, *J. Am. Chem. Soc.* **2020**, *142*, 9106.
[19] Y. Ji, T. Chakraborty, S. V. Wegner, *ACS Nano.* **2023**, *17*, 8992.
[20] B. C. Buddingh', J. Elzinga, J. C. M. van Hest, *Nat. Commun.* **2020**, *11*, 1652.
[21] Y. Elani, *Angew. Chem., Int. Ed.* **2021**, *60*, 5602.
[22] X. Wang, L. Tian, H. Du, M. Li, W. Mu, B. W. Drinkwater, X. Han, S. Mann, *Chem. Sci.* **2019**, *10*, 9446.
[23] J. M. Smith, D. Hartmann, M. J. Booth, *Nat. Chem. Biol.* **2023**, *19*, 1138.
[24] H. Niederholtmeyer, C. Chaggan, N. K. Devaraj, *Nat. Commun.* **2018**, *9*, 5027.
[25] Ö. D. Toparlak, J. Zasso, S. Bridi, M. Dalla Serra, P. Macchi, L. Conti, M.-L. Baudet, S. S. Mansy, *Sci. Adv.* **2020**, *6*, 4920.
[26] G. Chen, R. Levin, S. Landau, M. Kaduri, O. Adir, I. Ianovici, N. Krinsky, O. Doppelt-Flikshtain, J. Shklover, J. Shainsky-Roitman, S. Levenberg, A. Schroeder, *Proc. Natl. Acad. Sci. USA* **2022**, *119*, e2207525119.
[27] Z. Chen, J. Wang, W. Sun, E. Archibong, A. R. Kahkoska, X. Zhang, Y. Lu, F. S. Ligler, J. B. Buse, Z. Gu, *Nat. Chem. Biol.* **2018**, *14*, 86.
[28] U. Park, M. S. Lee, J. Jeon, S. Lee, M. P. Hwang, Y. Wang, H. S. Yang, K. Kim, *Acta Biomater.* **2019**, *90*, 179.
[29] M. P. Hwang, R. J. Fecek, T. Qin, W. J. Storkus, Y. Wang, *J. Control. Release.* **2020**, *318*, 270.
[30] Z. Lin, T. Beneyton, J. C. Baret, N. Martin, *Small. Methods.* **2023**, *7*, e2300496.
[31] S. Liu, Y. Zhang, M. Li, L. Xiong, Z. Zhang, X. Yang, X. He, K. Wang, J. Liu, S. Mann, *Nat. Chem.* **2020**, *12*, 1165.
[32] F. Pir Cakmak, A. M. Marianelli, C. D. Keating, *Langmuir* **2021**, *37*, 10366.
[33] A. F. Mason, B. C. Buddingh, D. S. Williams, J. C. M. Van Hest, *J. Am. Chem. Soc.* **2017**, *139*, 17309.

[34] T. Y. Dora Tang, C. Rohaida Che Hak, A. J. Thompson, M. K. Kuimova, D. S. Williams, A. W. Perriman, S. Mann, *Nat. Chem.* **2014**, *6*, 527.
[35] S. F. Banani, H. O. Lee, A. A. Hyman, M. K. Rosen, *Nat. Rev. Mol. Cell. Biol.* **2017**, *18*, 285.
[36] W. C. Blocher McTigue, S. L. Perry, *Soft. Matter.* **2019**, *15*, 3089.
[37] A. F. Mason, N. A. Yewdall, P. L. W. Welzen, J. Shao, M. Van Stevendaal, J. C. M. V. Hest, D. S. Williams, L. K. E. A. Abdelmohsen, *ACS Cent. Sci.* **2019**, *5*, 1360.
[38] R. A. Kapelner, A. C. Obermeyer, *Chem. Sci.* **2019**, *10*, 2700.
[39] T. Mashima, M. H. M. E. van Stevendaal, F. R. A. Cornelissens, A. F. Mason, B. J. H. M. Rosier, W. J. Altenburg, K. Oohora, S. Hirayama, T. Hayashi, J. C. M. van Hest, L. Brunsveld, *Angew. Chem. Int. Ed.* **2022**, *61*, e202115041.
[40] W. J. Altenburg, N. A. Yewdall, D. F. M. Vervoort, M. H. M. E. van Stevendaal, A. F. Mason, J. C. M. van Hest, *Nat. Commun.* **2020**, *11*, 6282.
[41] D. P. Nguyen, M. Mahesh, S. J. Elsässer, S. M. Hancock, C. Uttamapinant, J. W. Chin, *J. Am. Chem. Soc.* **2014**, *136*, 2240.
[42] R. B. Kapust, J. Tözsér, J. D. Fox, D. E. Anderson, S. Cherry, T. D. Copeland, D. S. Waugh, *Protein. Eng.* **2001**, *14*, 993.
[43] P. Rathert, T. Raskó, M. Roth, K. Ślaska-Kiss, A. Pingoud, A. Kiss, A. Jeltsch, *ChemBioChem* **2007**, *8*, 202.
[44] J. Phan, A. Zdanov, A. G. Evdokimov, J. E. Tropea, H. K. Peters, R. B. Kapust, M. Li, A. Wlodawer, D. S. Waugh, *J. Biol. Chem.* **2002**, *277*, 50564.
[45] C. M. Nunn, M. Jeeves, M. J. Cliff, G. T. Urquhart, R. R. George, L. H. Chao, Y. Tscuchia, S. Djordjevic, *J. Mol. Biol.* **2005**, *350*, 145.
[46] C. E. Correnti, M. M. Gewe, C. Mehlin, A. D. Bandaranayake, W. A. Johnsen, P. B. Rupert, M. Y. Brusniak, M. Clarke, S. E. Burke, W. De Van Der Schueren, K. Pilat, S. M. Turnbaugh, D. May, A. Watson, M. K. Chan, C. D. Bahl, J. M. Olson, R. K. Strong, *Nat. Struct. Mol. Biol.* **2018**, *25*, 270.
[47] P. T. Wingfield, *Curr. Protoc. Protein. Sci.* **2017**, *88*, 6.14.1.
[48] M. Molzan, S. Kasper, L. Röglin, M. Skwarczynska, T. Sassa, T. Inoue, F. Breitenbuecher, J. Ohkanda, N. Kato, M. Schuler, C. Ottmann, *ACS Chem. Biol.* **2013**, *8*, 1869.
[49] T. W. van Veldhuisen, W. J. Altenburg, M. A. M. Verwiel, L. J. M. Lemmens, A. F. Mason, M. Merkx, L. Brunsveld, J. C. M. van Hest, *Adv. Mater.* **2023**, *35*, 2300947.
[50] A. Hazegh Nikroo, L. J. M. Lemmens, T. Wezeman, C. Ottmann, M. Merkx, L. Brunsveld, *ACS Synth. Biol.* **2022**, *11*, 2464.
[51] S. Wu, H. Luo, H. Wang, W. Zhao, Q. Hu, Y. Yang, *Biochem. Biophys. Res. Commun.* **2016**, *478*, 1268.